IEEE Access
Multidisciplinary | Rapid Review | Open Access Journal

Received December 11, 2020, accepted December 17, 2020, date of publication December 23, 2020,
date of current version January 4, 2021.

Digital Object Identifier 10.1109/ACCESS.2020.3046720

Broadband Compact Circularly Polarized Spiral Antenna Array Fed by Printed Gap Waveguide for Millimeter-Wave Applications

ELHAM BAGHERNIA, (Graduate Student Member, IEEE), REZA MOVAHEDINIA, (Member, IEEE), AND ABDEL-RAZIK SEBAK, (Life Fellow, IEEE)
Department of Electrical and Computer Engineering, Concordia University, Montreal, QC H3G 1M8, Canada
Corresponding author: Elham Baghernia (e_bagher@encs.concordia.ca)

ABSTRACT This paper presents a new design for a wideband circularly polarized (CP) spiral antenna array fed by a differential aperture coupling. The differential excitation is realized by two vias located at the lateral sides of a transverse slot etched on the lower substrate. The proposed two-arm spiral antenna has a smaller size compared to conventional spiral antennas with several turns. The presented single radiating element provides the impedance bandwidth of ($|S11| < -10$ dB) 40.4% and 3-dB axial ratio (AR) of 23.2% with a peak RHCP gain of 7.2 dBic over the operating frequency band. To further enhance the AR bandwidth and the maximum gain, the presented CP spiral element is employed in a 2×2 sequential feeding arrangement. The sequential feeding network is implemented using the low-loss printed gap waveguide (PGW) line, which is compatible with low-cost printed circuit board (PCB) technology. A prototype of the proposed 2×2 antenna array is fabricated and measured experimentally. Measured results reveal that the designed antenna array has a wide impedance bandwidth of over 48.5%, the 3-dB AR bandwidth of 34.2%, and the 3-dB gain bandwidth of 32.4% with a maximum gain of 11.74 dBic and excellent radiation efficiency of 85% over the entire operating frequency band.

INDEX TERMS Spiral antenna, broadband antennas, circular polarization (CP), printed gap waveguide (PGW), sequential rotation feeding, printed circuit board (PCB), millimeter-wave (mm-wave).

I. INTRODUCTION

Circularly polarized (CP) antennas have attracted significant attention in millimeter-wave (mm-wave) wireless communication systems due to their distinct advantages of reducing polarization mismatch and suppression of multipath interference [1]. On the other hand, in order to keep up with the ever-increasing demand for the high data-rate transmission, antennas as vital components of every communication systems are needed to be broadband [2], [3]. Therefore, the wideband CP antenna is a promising candidate at mm-wave bands.

Various types of mm-wave CP antennas were designed in the literature, such as patch antenna [4], [5], slot antenna [6], magneto electric (ME) dipole antenna [7], [8], aperture antenna [9] and helix and spiral antennas [10], [11]. Among these antennas, traveling wave antennas are one of the desirable candidates that are able to provide stable radiation performance over wide frequency bandwidth. Traveling wave antennas refer to those antennas whose lengths are long enough to have the minimum reflected waves [12]. Spiral and helical antennas are classified into this category. Due to the 3D geometry of helical antennas, their fabrication in the mm-wave frequency band is quite challenging. The proposed helical antenna in [11], is fabricated by multilayer low-temperature co-fired ceramic (LTCC) technology. Despite the advantages of LTCC technology like compactness and lightweight, it is costly and complicated. Spiral antennas possess a planar structure and can be implemented using low-cost printed circuit board (PCB) technology. Therefore, spiral antennas are preferred to helical antennas in terms of the fabrication simplicity. However, there are two main problems in the realization of a spiral antenna at high frequencies, where compactness is a crucial requirement. The main problem with spiral antennas is that they need balun circuits to be excited in a balanced mode [13]. This problem becomes more severe in an antenna array configuration, in which

The associate editor coordinating the review of this manuscript and approving it for publication was Shah Nawaz Burokur.

balun circuits add more complexity to the whole structure. Another problem with the spiral antennas is that to fulfill the traveling wave requirements, the currents on spiral arms should have decaying current distribution [12]. This situation happens if the spiral is electrically large enough; otherwise, the reflected currents from the arms ends causing the total currents distribution to be standing waves, which in turn deteriorates the wideband characteristics of the AR and impedance matching [14]. Considering fabrication constraints and the size of spiral antenna with multiple turns, it is hard to keep element spacing in array configuration less than λ_0 (where λ_0 is the free space wavelength) at mm-wave frequencies and avoid the presence of grating lobes. Moreover, conventional approaches such as coating the arm ending with chip resistors [15] or terminating the spiral arms with zigzag sections [16] are not appropriate at mm-Wave frequency bands due to the severe loss at high frequencies and difficulties in fabrication, respectively. These problems hinder the usage of spiral antennas at high frequencies, despite their desirable wideband radiation performance.

Zhu *et al.* in [11] addressed these problems. To make the spiral antenna independent of balun circuits, spiral arms are differentially fed using two opposing vias located at the two sides of the coupling slot. Besides, to have the CP wave generation from the shorter spiral arms, their lengths are differed by $\lambda/4$ to create a 90° phase difference between the surface currents on both arms. However, perturbing the symmetry of the spiral antenna causes beam tilting in the radiation pattern. In this paper, we tried to tackle the problem of the large dimension of the spiral antenna without perturbing the spirals' symmetry.

To broaden the array AR bandwidth and improve the array CP purity, the sequential-rotation (SR) feed technique has extensively been used in literature. The SR feeding scheme has been implemented with different feeding technologies for mm-wave applications, including microstrip line (MSL) [17], [18], LTCC [19], and SIW [6], [20]. MSL was most popular at low frequencies due to such advantages as compactness, design flexibility, and low cost of fabrication. However, they usually suffer from radiation loss, which is more severe at high frequencies [21]. In addition, the parasitic radiation from microstrip feed networks has an adverse effect on the total radiation pattern of the antenna array. Radiation leakage and undesirable spurious radiation of the feed network is minimized in SIW since it is a self-package structure. However, they have some issues. Apart from a high dielectric loss at mm-wave frequencies, which makes the SIW less efficient compared to air traveling structures, it is not suitable for the realization of the SR feed network due to the large size of 3dB quadrature hybrid couplers and phase shifters. Recently, a multilayer aperture coupled approach is utilized to alleviate this problem [22]. However, the multilayer design adds more losses and difficulties in fabrication, particularly for large arrays. Printed gap waveguide (PGW) technology is a promising alternative for microstrip lines at high frequencies [23]–[25]. It's a compromise between the microstrip line and SIW as it is a package structure and suppresses the radiation loss and also has design flexibility, which is highly desirable for the implementation of the SR feeding networks.

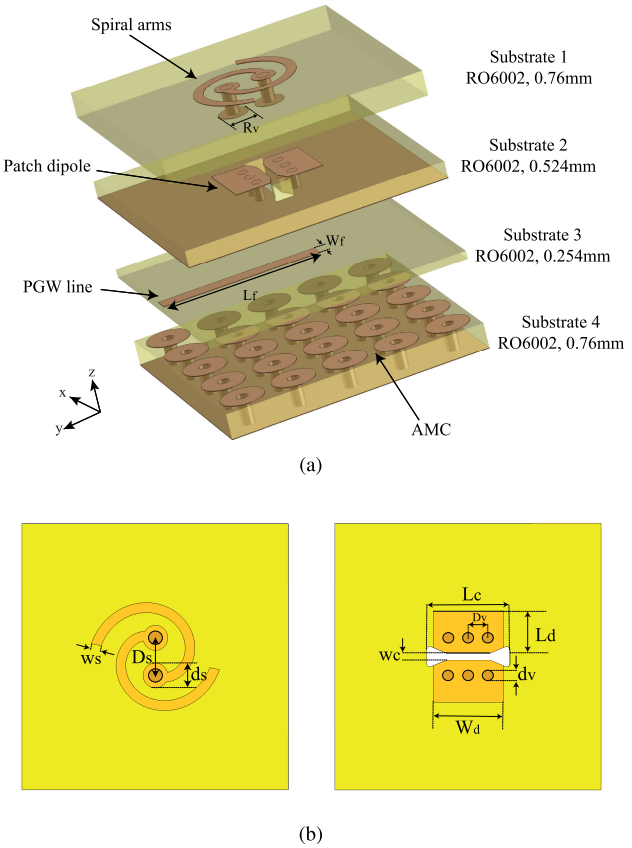

FIGURE 1. Geometry of the proposed antenna element. (a) Perspective view. (b) Top view.

In this paper, we propose a wideband and compact CP spiral antenna array fed by the PGW SR feeding structure. The proposed spiral antenna is relatively small and has less than one turn. The designed antenna array has been fabricated, and its performance is validated by measurement. The rest of this paper is organized as follows; Section II discusses the design principles of the proposed antenna structure and the PGW line. Section III presents the implementation of the antenna array, followed by the design of the PGW sequential feeding network. The experimental prototyping results and comparison with other similar works are illustrated in Section IV. Finally, Section V presents the conclusion of this paper.

II. REALIZATION OF THE PROPOSED CP SPIRAL ANTENNA

A. SINGLE RADIATING ELEMENT DESIGN

Fig. 1 illustrates the configuration of the proposed structure. It consists of a two-arm symmetrical spiral antenna on top of substrate 1 and two planar patches printed on substrate 2, which form a half-wavelength dipole. Both substrates are Rogers RO6002 with $\epsilon_r = 2.92$, $tan\delta = 0.0012$ and thicknesses of 0.762 mm and 0.528 mm from top to bottom, respectively. Therefore, the spiral antenna is located above a

TABLE 1. Dimension of the proposed single element (mm).

Parameter	W_f	L_f	W_s	D_s	d_s	L_c	W_c
Value	0.5	4.9	0.3	1.13	0.74	2.5	0.22
Parameter	W_d	L_d	d_v	D_v	R_v	a^*	θ^{**}_{end}
Value	2.1	1.25	0.3	0.6	0.89	0.276	4.51

* The unit is rad/mm.
** The unit is rad.

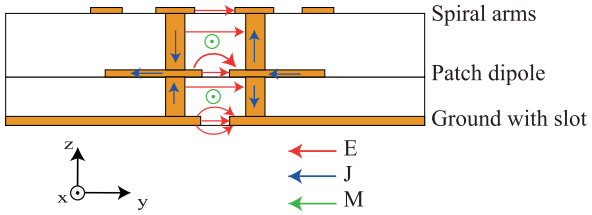

FIGURE 2. Cross section view of the proposed element with sketch of electric field, electric and magnetic currents.

conducting ground plane with a height of approximately $\lambda_g/4$ (is the guided wavelength in substrate 2 and 3) to ensure the unidirectional radiation pattern. The spiral arms constructed by the Archimedean spiral function of $r = a\theta + b$ in the polar coordinate system, where a is spiral constant, θ represents the winding angle, and b is the initial radius. Here b can be obtained by $0.5(D_s - w_c)$, where w_c is the width of the coupling slot, and D_s is center to center via distance on the top layer and is determined by fabrication constraints. The second arm of the spiral antenna is composed by rotation of the first arm by π rad. The winding angle of the spiral is increasing from 0 to 4.51 rad, and the spiral number of turns is N=0.83.

The spiral arms are fed differentially by two opposing vias located at both sides of a transverse slot, which is etched on a lower substrate. The length of the coupling slot is $\frac{\lambda_g}{2}$ where λ_g is the guided wavelength at the center frequency of 34 GHz. It is noted that two circular patches surround two vias on the bottom of substrate 1 to ensure good electrical contact between two vias and the patch dipoles on substrate 2.

The PGW feeding line is employed for the slot coupling. The shape of the slot is chosen to enhance the electromagnetic energy coupling between the slot and the PGW line. Detailed geometrical dimensions of the proposed structure are summarized in Table 1. The presented antenna generates RHCP (Right-hand Circular Polarization) due to the direction of spiral windings and differential phase excitation.

B. SINGLE ELEMENT OPERATING PRINCIPLES

To excite a two-arm spiral antenna in the fundamental mode, spiral arms must be excited with the same amplitude and 180° phase difference [13]. In our design, two vias located at the lateral sides of the slots etched on the top layer serves as a balun for the spiral arms. Fig. 2 illustrates the sketch of the electric field and electric currents on the cross section of the proposed structure. As it is shown, the electric currents on two vias of the top substrate are out of phase, which provides a differential feed for the spiral arms. The proposed spiral

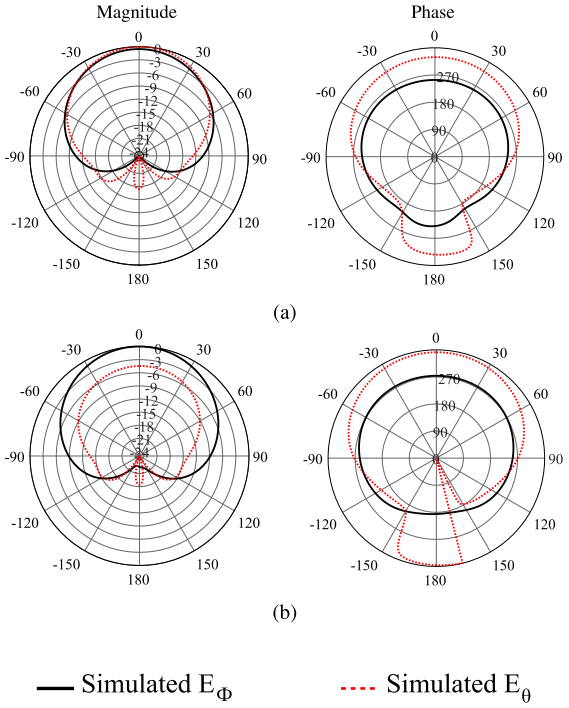

FIGURE 3. Magnitude and phase of E_θ and E_ϕ in the y-z plane at 34 GHz. (a) With patch dipole. (b) Without patch dipole.

antenna has a relatively small dimension with $\frac{D}{\lambda_0} = 0.41$. The polarization of an electrically small spiral antenna is highly elliptical due to the unequal magnitude of orthogonal electric currents at time intervals of t=T/4 (T is one period of time) on the spiral arms. The y-oriented patch dipole is placed under the spiral to reinforce the electric current along the y-direction. To better reveal the effect of the patch dipole on the CP performance, the magnitude and phase of far-field components of E_θ and E_ϕ in the y-z plane are plotted in Fig. 3. To provide a fair comparison, the distance of the spiral antenna from the ground plane is kept unchanged. As can be seen, for the case of without patch dipole $E_\phi > E_\theta$, which results in the elliptically polarized wave. However, adding the y-oriented patch dipole improves the E_θ components while the phase difference between E_θ and E_ϕ has remained almost constant at 90°.

To clarify the CP generation of the proposed structure, the simulated electric field distribution on a plane just above the top layer at t=0, T/4, T/2 and 3T/4 are plotted in Fig. 4. The black arrow represents the dominant direction of electric field components. Based on the orientation of the electric field, the co-polar vector is $E_{Co} = E_y - jE_x$, which confirms RHCP generation according to [26, eq.(2.21)].

C. PRINTED GAP WAVEGUIDE

The feedline is implemented using PGW technology. The PGW supports the propagation of the quasi-TEM wave in the air gap between the upper plate of the PGW structure and the microstrip line, which is placed above the artificial magnetic conductor (AMC). The AMC surface is realized by

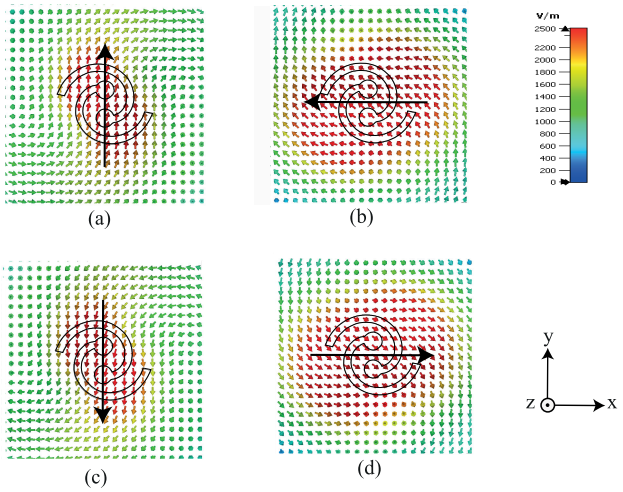

FIGURE 4. E-field distributions on the plane just above the top layer in a period of time at 34 GHz (a) t = 0. (b) t = T/4. (c) t = T/2. (d) t = 3T/4.

2D periodic EBG unit cells. However, the EBG structure can create the AMC boundary conditions over a limited frequency range, called stopband. Within the stopband, the electromagnetic wave follows the microstrip line, and propagation of any PEC–AMC parallel-plate modes is suppressed if the height of the air gap is less than a quarter of a free space wavelength [23]. The simulated dispersion diagram and the geometry of the unit cell are indicated in Fig. 5. The dispersion diagram, which shows the unit cell's stopband, is simulated through the Eigenmode solver of CST. The mushroom EBG unit cell is designed to cover the bandgap of 22.5-50 GHz based on the design guidelines of gap waveguides discussed in [24], [25]. RO6002 substrate with a loss tangent of 0.0009 and dielectric constant of 2.94 and thickness of 0.76 mm and 0.25 mm are used to print mushroom unit cell and metallic microstrip line. Fig. 6 (a) depicted the PGW section geometry, which consists of 3 rows of the unit cell on lateral sides of the printed microstrip line. By introducing a metallic microstrip between the PEC-AMC plates, a quasi-TEM mode can propagate within the bandgap frequency band, as shown in Fig. 6 (b). As can be seen from this figure, the bandgap of the PGW structure is from 22.9-46.3 GHz. It is noted that the PGW bandgap frequency range must cover the operational bandwidth of the designed antenna with margins.

Generally, the PGW line's width is larger than the microstrip line, which leads to a smaller conductive loss. Here, the width of PGW is chosen to provide characteristic impedance of 75Ω to provide a better matching for the high input impedance of the spiral antenna.

D. PERFORMANCE

The simulated reflection coefficient, AR, and gain of the proposed antenna are shown in Fig. 7 and Fig. 8, respectively. The presented single element has −15 dB impedance bandwidth of 37.2% ranging from 28.13 GHz to 41 GHz, 3-dB AR bandwidth of 23.2% ranging from 30.6 GHz to

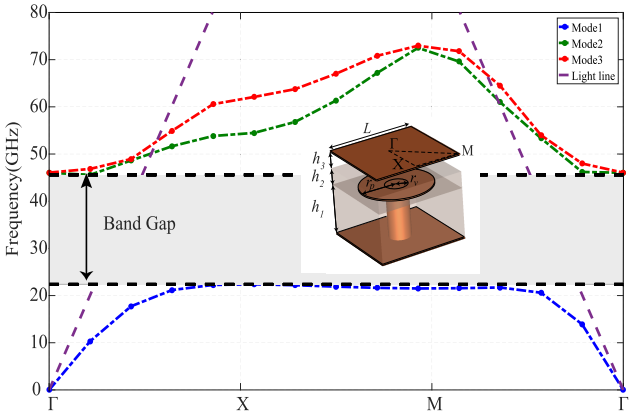

FIGURE 5. Dispersion diagram of the designed unitcell (with L = 1.6mm, r_p = 0.65mm, r_v = 0.4 mm, h_1 = 0.76mm, h_2 = h_3 = 0.254 mm).

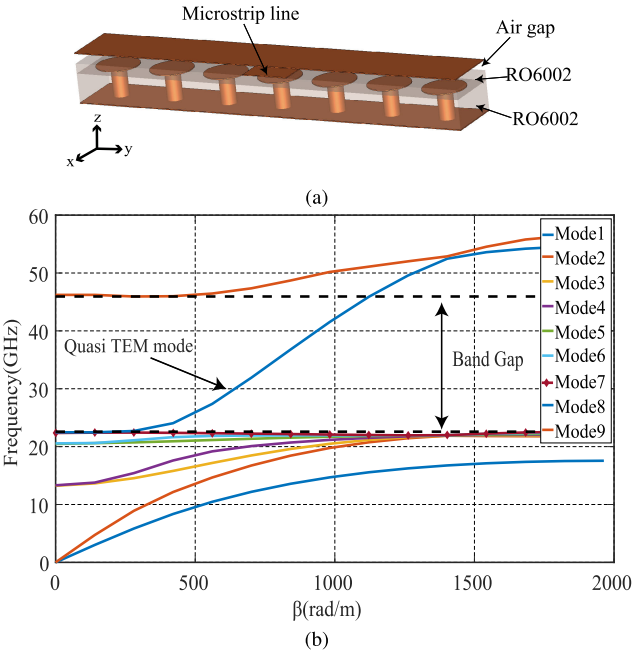

FIGURE 6. (a) PGW section. (b) Dispersion diagram of PGW section.

38.62 GHz and maximum RHCP gain of 7.2 dBic in the broadside direction. Fig. 9 presents the simulated normalized radiation pattern of the proposed structure in principal planes at 34 GHz. It can be observed from Fig. 9 that the proposed CP element exhibits low cross-polarization of −18.5 dB in broadside direction.

III. CIRCULARLY POLARIZED ANTENNA ARRAY

A. 2×2 ARRAY

The geometry of the 2×2 CP spiral antenna array is shown in Fig. 10. It consists of 3 main parts: (1) sequential feeding network on the bottom layer, (2) patch dipoles on the middle layer (3) spiral antenna on the top layer. The spacing between antenna elements is 0.85 λ_0 (λ_0 corresponds to the highest frequency in the operating band) to avoid the generation

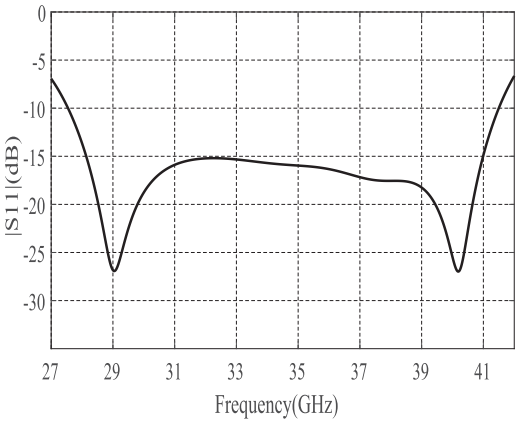

FIGURE 7. Simulated reflection coefficient of the proposed single antenna.

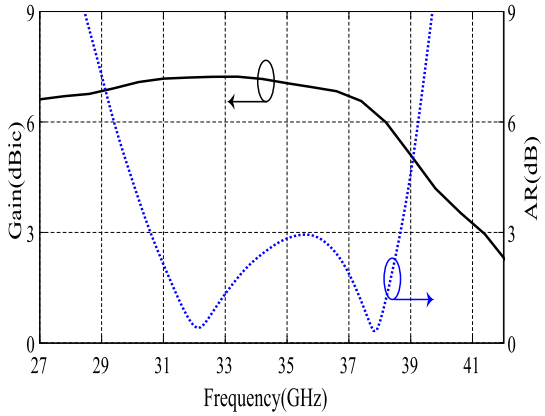

FIGURE 8. Simulated AR and RHCP Gain of the proposed single antenna.

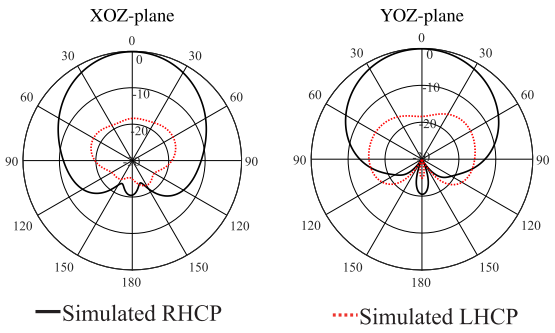

FIGURE 9. Simulated normalized radiation pattern of proposed single antenna at 34 GHz in the principal planes (xoz and yoz).

of grating lobes. The sequential feeding network is realized using PGW and will be further explained in the next part. A transition from the PGW line to the MS line is designed for the sake of measurement.

B. FEEDING NETWORK

The SR feed technique is a well-known method to broaden the AR bandwidth in which antenna elements undergo both progressive phase difference and physical rotation. This method can be applied to both LP and CP radiating

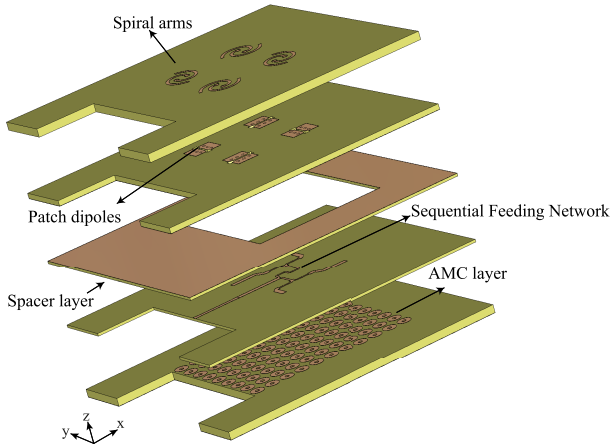

FIGURE 10. Proposed antenna array structure.

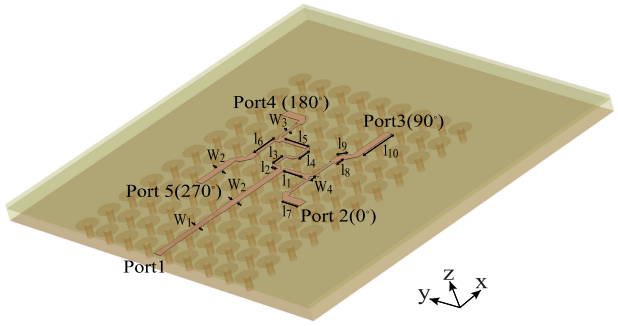

FIGURE 11. Sequential feeding network implemented by PGW.

TABLE 2. Dimension of the proposed sequential feeding Network (mm).

Parameter	W_1	W_2	W_3	W_4	l_1	l_2	l_3
Value	0.3	0.48	0.2	0.48	1.56	0.46	0.85
Parameter	l_4	l_5	l_6	l_7	l_8	l_9	l_{10}
Value	0.85	0.89	2.04	1.4	0.52	0.7	2.55

elements [17], [27], [28]. However, CP radiating element fed by the SR feed technique exhibits higher CP purity and wider AR bandwidth. It is worth mentioning that the employment of a corporate feed network that applies an equal phase to each antenna element in an array configuration usually deteriorates the CP performance of the whole antenna. In [7], the designed magneto electric antenna achieved the 3-dB AR bandwidth of 25.9%. But, for an 8×8 full-corporate substrate integrated waveguide (SIW) fed antenna array based on the proposed magneto electric (ME) dipole antenna element, the 3-dB AR bandwidth was reduced to 16.5%. The schematic of the designed sequential feeding network is plotted in Fig. 11, and its corresponding detailed dimensions are listed in Table 2. Since the single radiating element generates RHCP, the rotation and phase increment of the designed sequentially rotated feeding is in an anticlockwise direction. The required 90° phase difference is realized using a quarter length of PGW lines. It should be noted that the phase and amplitude error

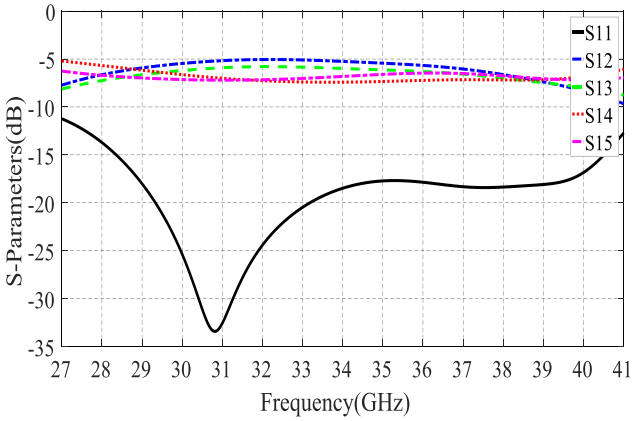

FIGURE 12. Simulated S-parameters of the designed sequential feeding network.

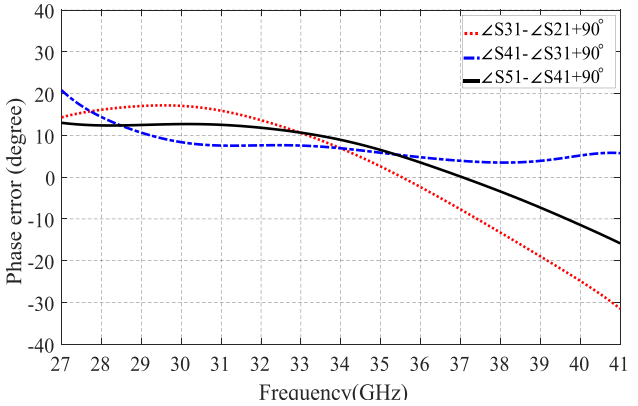

FIGURE 13. Simulated phase error between the subsequent ports of the designed sequential feeding network.

resulting from delay PGW lines, limit the operating bandwidth of the designed antenna array. To alleviate this problem, a metamaterial-based sequential feeding network is introduced in [29]. However, the lumped elements adopted in the metamaterial line can cause strong parasitic effects at high frequencies.

The simulated results of power dividing and phase error of the sequential feed network are shown in Fig.12 and Fig.13, respectively. The phase error (phase deviation from 90°) of the designed sequential feeding is less than 30° with the operating frequency band, and the maximum insertion loss is −7.4 dB.

IV. MEASURED AND SIMULATED ARRAY PERFORMANCE

A. FABRICATION AND MEASUREMENT

The proposed CP antenna array is fabricated and measured for performance verification. The photograph of the fabricated antenna prototype is plotted in Fig.14. First, each layer is fabricated using low-cost PCB manufacturing technology; then, all layers are stacked on top of each other using adhesive epoxy glue. It should be noted that the existence of the glue with material properties of $\epsilon_r = 3.5$, loss tangent=0.03, and thickness of $5\mu m$ is considered during the simulation process.

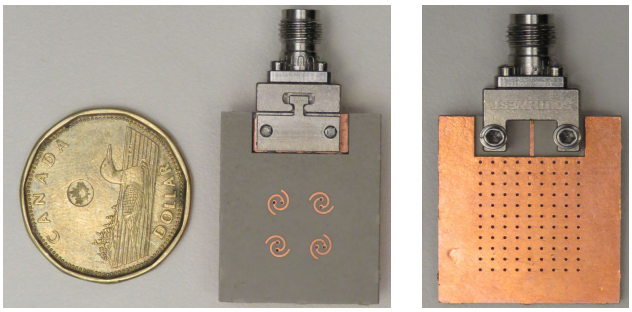

FIGURE 14. Photographs of fabricated proposed antenna arrays. (a) Top view. (b) Bottom view.

FIGURE 15. Radiation pattern measurement setup.

A 2.4 mm Southwest end launch connector is connected to the input port of the antenna for the sake of measurement. The overall dimension of the prototype antenna is 27.8 mm × 23.8 mm × 2.5 mm or $3.15\lambda_0 \times 2.7\lambda_0 \times 0.28\lambda_0$, where λ_0 is the wavelength in free space.

The radiation performance of the designed antenna array is measured using the far-field measurement setup shown in Fig. 15. As can be seen, an LP standard horn antenna is employed as a transmitting antenna. The gain of the designed CP array is obtained in two steps: first measuring the LP gain using the conventional gain comparing method and then applying the gain correction factor to get the CP gain as follows [30]:

$$G_{AUT}(dBic) = G_l + 3 + G_c \tag{1}$$

where G_l is the LP gain obtained from measurement and G_c is the gain correction factor calculated by:

$$G_c(dB) = 20log_{10}(0.5(1 + 10^{(\frac{-AR(dB)}{20})})) \tag{2}$$

For the pure CP antenna (with AR(dB)=0), $G_c = 0$ therefore, the 3 dB gain increase is required to convert the LP gain to the CP gain.

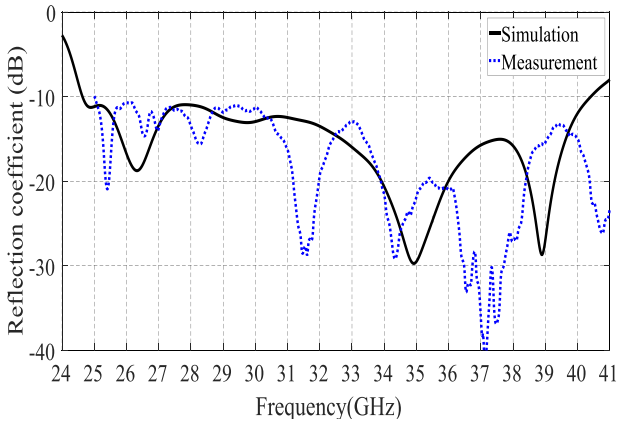

FIGURE 16. Simulated and measured reflection coefficient of the proposed antenna array.

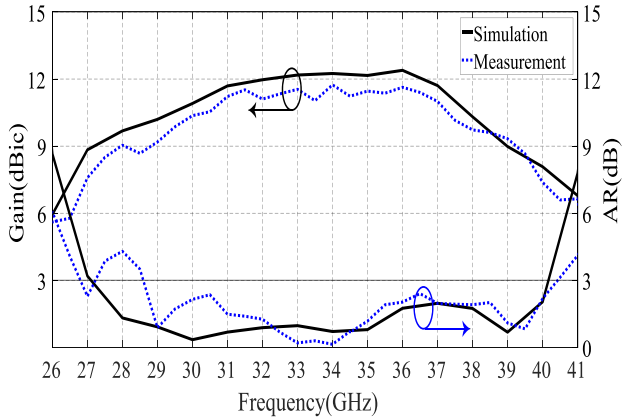

FIGURE 17. Simulated and measured RHCP gain and AR of the proposed antenna array.

B. EXPERIMENTAL RESULTS

The reflection coefficient of the fabricated antenna array was measured by the mm-wave phase network analyzer (N5227A). Fig. 16 compares the simulated and measured reflection coefficient of the proposed antenna array. Measured and simulated results indicate that the designed antenna has a wide impedance bandwidth. Measured and simulated matching impedance (i.e., $|S11| < -10dB$) cover the bandwidths of greater than 48.5% (25.03 GHz-41 GHz) and 48.6% (24.6 GHz- 40.4 GHz), respectively. The discrepancy between simulated and measured results for the impedance matching can be caused by the following factors: 1) smaller height of the air gap, which results in a wider matched bandwidth for the proposed antenna array; 2) the thickness of the glue, which changes the resonance frequency; 3) fabrication error in positioning vias on the top layer that leads to the resonance frequency shift, and 4) measurement errors. The simulated and measured AR and gain are plotted in Fig. 17. The measured AR has the 3-dB bandwidth of 34.2% (28.6 GHz – 40.4 GHz) and simulated 3-dB bandwidth of 38.9 % (27.1 GHz – 40.2 GHz). The maximum measurement gain is 11.74 dBic at 34 GHz. The maximum measured gain is slightly lower than the simulated gain, which could be due to the loss introduced by the connector and glue used to stack the fabricated layers.

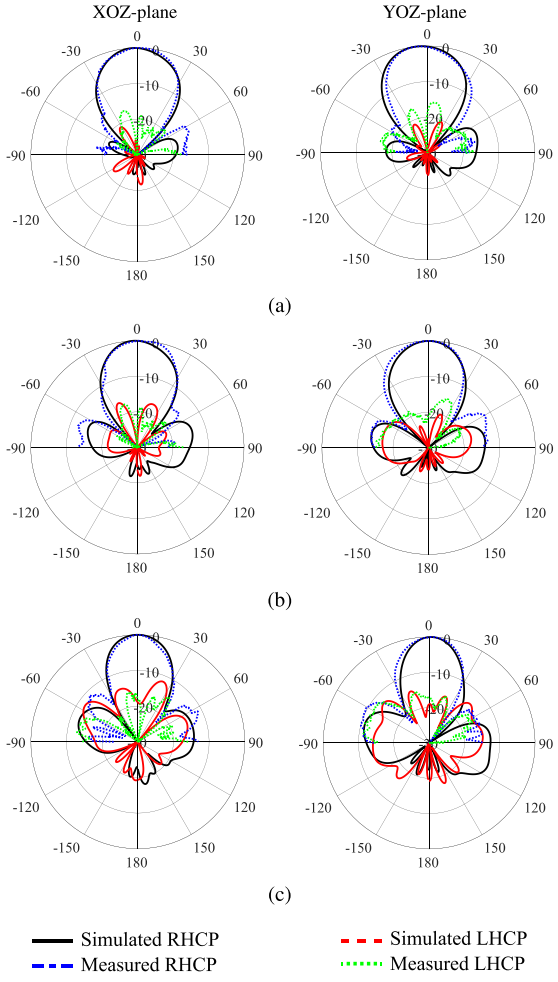

FIGURE 18. Simulated 2-D radiation patterns of the proposed antenna array at (a) 31 GHz,(b) 34 GHz, and (c) 37 GHz.

The simulated and measured normalized radiation patterns in two principal planes for three different frequencies of 31 GHz, 34 GHz, and 37 GHz are shown in Fig. 18. As can be seen from this figure, the measurement results agree well with the simulated results. The maximum measured cross-polarization level (i.e., LHCP) at 34 GHz is around −21.3 dB at both XOZ and YOZ planes. Fig. 19 indicates the simulated radiation efficiency for both proposed single antenna element and 2×2 antenna array. As shown in this figure, the simulated radiation efficiency of the proposed antenna array exceeds 85% over the entire frequency bandwidth due to the implementation of the feeding network with a low-loss and self-package technology of PGW.

The proposed 2×2 antenna array is suitable to be used as a subarray for building larger antenna array structures. It is expected that broader AR bandwidth is obtained with a larger SR antenna array. Each round of SR suppresses the cross-polarization level further, and as a result, the AR bandwidth

TABLE 3. Comparison between the proposed mm wave CP antenna array and some related works in the references.

Ref.	Element	Fab. Tech.	Freq.	Element Num.	Feeding Network	Size (λ_0^3)	Imp. BW %	AR BW %	Gain BW %	Peak Gain (dBic)	Radiation Efficiency %
[10]	Helical	LTCC	60	4×4	Full corporate (Strip line)	2.4×2.0×0.40	22	20	15.1	15.2	54.9
[11]	Spiral	PCB	60	4×4	Sequential (SIW)	4.9×4.9×0.49	14.1	21.1	16.4	19.5	>77
[6]	Slot	PCB	28	2×2	Sequential (SIW)	3.46×3.46×0.09	23.3	7.7	7	10.78	NG*
[31]	Patch	PCB	26	2×2	Sequential (SIGW)	3.9×3.5×0.24	25.6	19	25	11.53	NG*
[32]	Aperture	PCB	30	2×2	Differential (PGW)	6.1×4.9×0.16	15.6	10	14	13.5	>84
[33]	Slot spiral	PCB	38	2×2	Sequential (PGW)	4.4×4.4×0.25	23.7	22.5	21	12.3	>82
[34]	ME-dipole	PCB	27	4×4	Sequential (SIW)	7.0 ×5.0×0.42	27.7	27.8	25.3	20.2	78
This work	Spiral	PCB	34	2×2	Sequential (PGW)	3.15×2.7×0.28	> 48.5	34.2	32.4	11.74	>85

*The numerical data is not given in the referenced paper.

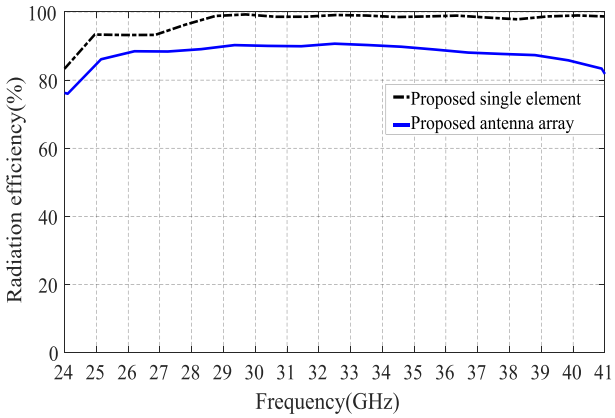

FIGURE 19. Simulated radiation efficiency of the proposed single element and antenna array.

is enhanced [26]:

$$AR(dB) = 20log\left|\frac{1+|\frac{E_{xp}}{E_{co}}|}{1-|\frac{E_{xp}}{E_{co}}|}\right| \quad (3)$$

where E_{xp} and E_{co} represent cross- and co-polar electric field components, respectively. The effect of each round of SR on co- and cross-polar components of the electric field is given in the appendix.

C. COMPARISON AND DISCUSSION

Table 3 compares the measured results of the proposed mm-wave CP antenna array with some previously reported works in literature in terms of the size, impedance bandwidth, CP performance, gain, and total efficiency. The total sizes of the antenna arrays are considered for comparison. Except for the reported antenna array in [10], all the antennas listed in Table 3 are fabricated using low-cost PCB technology. The presented antenna array in [11] has a wide AR bandwidth. However, the impedance bandwidth is limited due to the usage of the asymmetrical spiral antenna as a radiating element. Despite having a broad impedance bandwidth of 23.3%, the proposed design in [6] suffers from a narrow AR bandwidth. Compared to antenna arrays fed by SIW and MS lines, PGW-fed antennas exhibit higher radiation efficiency [32], [33]. Therefore, PGW technology is a good alternative for the implementation of feeding networks at mm-wave frequencies. Since the differential feed network in [32] is realized using two layers of PGW, including two thin air gaps, it has more difficult fabrication compared to our work. Overall, as can be seen from Table 3, the proposed CP antenna array archives better reflection coefficient, AR, and gain bandwidth with high radiation efficiency compared to the other CP antenna arrays listed in this table.

V. CONCLUSION

We presented a wideband compact CP spiral antenna array for mm-wave applications. The patch dipole beneath the spiral arms helps the spiral to shrink but at the expense of adding one layer. Also, the connecting vias to the patch dipole provide a 180° phase difference for the spiral arms to be excited with its fundamental mode. To further increase the AR bandwidth,

the proposed single element is employed in a SR feeding network. The sequential feeding is implemented using PGW technology, which benefits from the design flexibility of MS lines and, at the same time, having low dispersion. The prototype of the planar CP antenna array has been designed, fabricated and measured. The measured results are in good agreement with the simulated results. Based on the measured results, the fabricated antenna array has a wide impedance bandwidth of more than 48.5%, 3-dB AR of 34.2% and 3-dB gain bandwidth of 32.4% with a maximum gain of 11.74 dBic over the operating frequency bandwidth. In addition, the proposed antenna array exhibits high radiation efficiency.

APPENDIX. ELECTRIC FIELD OF N-ELEMENT SEQUENTIALLY ROTATED ANTENNA ARRAY

The electric field can be expressed in terms of co- and cross-polar components [26]:

$$\vec{E} = (E_{co}\hat{e}_{co} + E_{xp}\hat{e}_{xp})e^{-jkz} \tag{4}$$

where $\hat{e_{co}}$ and $\hat{e_{xp}}$ are co-polar and cross-polar unit vectors, respectively. Co- and cross-polar unit vectors for RHCP, are defined as:

$$\hat{e}_{co} = \frac{\hat{x} - j\hat{y}}{\sqrt{2}} \tag{5}$$

$$\hat{e}_{xp} = \frac{\hat{x} + j\hat{y}}{\sqrt{2}} \tag{6}$$

To find the rotated electric field components at the broadside direction, we can use 2-D Rodrigues' rotation formula:

$$\vec{r'} = cos\beta\vec{r} + sin\beta(\hat{n} \times \vec{r}) \tag{7}$$

where $\vec{r'}$ is the rotated position vector, $\vec{r}$ is the position vector, β is the angle of rotation and $\vec{n}$ is the axis of rotation. Therefore, the electric field of n_{th} antenna element rotated around the z-axis by angle of $n\beta$ can be obtained as:

$$\begin{aligned}\vec{E}'_n &= cos(n\beta)\vec{E} + sin(n\beta)(\hat{z} \times \vec{E}) \\ \vec{E}'_n &= (e^{jn\beta}E_{co}\hat{e}_{co} + e^{-jn\beta}E_{xp}\hat{e}_{xp})e^{-jkz}\end{aligned} \tag{8}$$

After applying the phase shift of $n\alpha$ to each antenna element, the electric field can be written as:

$$\vec{E}''_n = e^{jn\alpha}\vec{E}'_n \tag{9}$$

$$\vec{E}''_n = (e^{jn(\beta+\alpha)}E_{co}\hat{e}_{co} + e^{-jn(\beta-\alpha)}E_{xp}\hat{e}_{xp})e^{-jkz} \tag{10}$$

Finally, the total electric field in the boresight direction produced by N sequentially rotated antenna elements is calculated as:

$$\begin{aligned}\vec{E}^t &= \vec{E}^t_{co} + \vec{E}^t_{xp} = \sum_{n=0}^{N-1}\vec{E}''_n \\ &= (\sum_{n=0}^{N-1} e^{jn(\beta+\alpha)}E_{co}\hat{e}_{co} + \sum_{n=0}^{N-1} e^{-jn(\beta-\alpha)}E_{xp}\hat{e}_{xp})e^{-jkz}\end{aligned} \tag{11}$$

For N sequentially rotated antenna elements generating RHCP radiation, geometrical phase rotation is in an anti-clockwise direction ($\beta > 0$), considering $\alpha = -\beta$, the total co- and cross-polar components of the electric field become as follows:

$$\vec{E}^t_{co} = NE_{co}\hat{e}_{co} \tag{12}$$

$$\vec{E}^t_{xp} = 0 \tag{13}$$

REFERENCES

[1] S. S. Gao, Q. Luo, and F. Zhu, "Introduction to circularly polarized antennas," in *Circularly Polarized Antennas*, 2014, pp. 1–2.
[2] T. S. Rappaport, *Wireless Communications: Principles and Practice*, vol. 2. Upper Saddle River, NJ, USA: Prentice-Hall, 1996.
[3] L. Wei, R. Hu, Y. Qian, and G. Wu, "Key elements to enable millimeter wave communications for 5G wireless systems," *IEEE Wireless Commun.*, vol. 21, no. 6, pp. 136–143, Dec. 2014.
[4] M. Li and K.-M. Luk, "Low-cost wideband microstrip antenna array for 60-GHz applications," *IEEE Trans. Antennas Propag.*, vol. 62, no. 6, pp. 3012–3018, Jun. 2014.
[5] A. B. Guntupalli and K. Wu, "60-GHz circularly polarized antenna array made in low-cost fabrication process," *IEEE Antennas Wireless Propag. Lett.*, vol. 13, pp. 864–867, 2014.
[6] Q. Wu, H. Wang, C. Yu, and W. Hong, "Low-profile circularly polarized cavity-backed antennas using SIW techniques," *IEEE Trans. Antennas Propag.*, vol. 64, no. 7, pp. 2832–2839, Jul. 2016.
[7] Y. Li and K.-M. Luk, "A 60-GHz wideband circularly polarized aperture-coupled magneto-electric dipole antenna array," *IEEE Trans. Antennas Propag.*, vol. 64, no. 4, pp. 1325–1333, Apr. 2016.
[8] A. Dadgarpour, M. Sharifi Sorkherizi, and A. A. Kishk, "High-efficient circularly polarized magnetoelectric dipole antenna for 5G applications using dual-polarized split-ring resonator lens," *IEEE Trans. Antennas Propag.*, vol. 65, no. 8, pp. 4263–4267, Aug. 2017.
[9] D. J. Bisharat, S. Liao, and Q. Xue, "High gain and low cost differentially fed circularly polarized planar aperture antenna for broadband millimeter-wave applications," *IEEE Trans. Antennas Propag.*, vol. 64, no. 1, pp. 33–42, Jan. 2016.
[10] C. Liu, Y.-X. Guo, X. Bao, and S.-Q. Xiao, "60-GHz LTCC integrated circularly polarized helical antenna array," *IEEE Trans. Antennas Propag.*, vol. 60, no. 3, pp. 1329–1335, Mar. 2012.
[11] Q. Zhu, K.-B. Ng, and C. H. Chan, "Printed circularly polarized spiral antenna array for millimeter-wave applications," *IEEE Trans. Antennas Propag.*, vol. 65, no. 2, pp. 636–643, Feb. 2017.
[12] C. A. Balanis, "Traveling wave and broadband antennas," in *Antenna Theory: Analysis and Design*. Hoboken, NJ, USA: Wiley, 2016, ch. 10, pp. 549–602.
[13] H. Nakano, T. Igarashi, H. Oyanagi, Y. Iitsuka, and J. Yamauchi, "Unbalanced-mode spiral antenna backed by an extremely shallow cavity," *IEEE Trans. Antennas Propag.*, vol. 57, no. 6, pp. 1625–1633, Jun. 2009.
[14] H. Nakano, K. Nogami, S. Arai, H. Mimaki, and J. Yamauchi, "A spiral antenna backed by a conducting plane reflector," *IEEE Trans. Antennas Propag.*, vol. 34, no. 6, pp. 791–796, Jun. 1986.
[15] L. Schreider, X. Begaud, M. Soiron, and B. Perpere, "Archimedean microstrip spiral antenna loaded by chip resistors inside substrate," in *Proc. IEEE Antennas Propag. Soc. Symp.*, Jun. 2004, pp. 1066–1069.
[16] H. Nakano and J. Yamauchi, "Sunflower spiral antenna," in *Proc. Antennas Propag. Soc. Int. Symp.*, Jun. 1980, pp. 709–712.
[17] S.-K. Lin and Y.-C. Lin, "A compact sequential-phase feed using uniform transmission lines for circularly polarized sequential-rotation arrays," *IEEE Trans. Antennas Propag.*, vol. 59, no. 7, pp. 2721–2724, Jul. 2011.
[18] Z. Gan, Z. Tu, Z. Xie, Q. Chu, and Y. Yao, "Compact wideband circularly polarized microstrip antenna array for 45 GHz application," *IEEE Trans. Antennas Propag.*, vol. 66, no. 11, pp. 6388–6392, Nov. 2018.
[19] M. Du, Y. Dong, J. Xu, and X. Ding, "35-GHz wideband circularly polarized patch array on LTCC," *IEEE Trans. Antennas Propag.*, vol. 65, no. 6, pp. 3235–3240, Jun. 2017.
[20] D.-F. Guan, C. Ding, Z.-P. Qian, Y.-S. Zhang, Y. Jay Guo, and K. Gong, "Broadband high-gain SIW cavity-backed circular-polarized array antenna," *IEEE Trans. Antennas Propag.*, vol. 64, no. 4, pp. 1493–1497, Apr. 2016.
[21] E. J. Denlinger, "Losses of microstrip lines," *IEEE Trans. Microw. Theory Techn.*, vol. MTT-28, no. 6, pp. 513–522, Jun. 1980.

[22] W. M. Abdel-Wahab, A.-S. Hussam, S. Safavi-Naeini, and Y. Wang, "Circularly polarized SIW-integrated DRA for low cost millimeter wave systems," in *Proc. Global Symp. Millimeter-Waves (GSMM)*, May 2015, pp. 1–3.
[23] P. S. Kildal, E. Alfonso, A. Valero-Nogueira, and E.Rajo-Iglesias, "Local metamaterial-based waveguides in gaps between parallel metal plates," *IEEE Antennas Wireless Propag. Lett.*, vol. 8, pp. 84–87, 2009.
[24] P. S. Kildal, A. U. Zaman, E. Rajo-Iglesias, E. Alfonso, and A. Valero-Nogueira, "Design and experimental verification of ridge gap waveguide in bed of nails for parallel-platemode suppression," *IET Microw., Antennas, Propag.*, vol. 5, no. 3, pp. 262–270, Feb. 2011.
[25] M. Sharifi Sorkherizi and A. A. Kishk, "Fully printed gap waveguide with facilitated design properties," *IEEE Microw. Wireless Compon. Lett.*, vol. 26, no. 9, pp. 657–659, Sep. 2016.
[26] P.-S. Kildal, "Characterization of directive antennas," in *Foundations of Antenna Engineering: A Unified Approach for Line-of-Sight and Multipath*. Norwood, MA, USA: Artech House, 2015, ch. 2, pp. 24–27.
[27] S.-L.-S. Yang, R. Chair, A. A. Kishk, K.-F. Lee, and K.-M. Luk, "Study on sequential feeding networks for subarrays of circularly polarized elliptical dielectric resonator antenna," *IEEE Trans. Antennas Propag.*, vol. 55, no. 2, pp. 321–333, Feb. 2007.
[28] Y. Li, Z. Zhang, and Z. Feng, "A sequential-phase feed using a circularly polarized shorted loop structure," *IEEE Trans. Antennas Propag.*, vol. 61, no. 3, pp. 1443–1447, Mar. 2013.
[29] K. L. Chung, "High-performance circularly polarized antenna array using metamaterial-line based feed network," *IEEE Trans. Antennas Propag.*, vol. 61, no. 12, pp. 6233–6237, Dec. 2013.
[30] B. Yen Toh, R. Cahill, and V. F. Fusco, "Understanding and measuring circular polarization," *IEEE Trans. Educ.*, vol. 46, no. 3, pp. 313–318, Aug. 2003.
[31] C. Ma, Z.-H. Ma, and X. Zhang, "Millimeter-wave circularly polarized array antenna using substrate-integrated gap waveguide sequentially rotating phase feed," *IEEE Antennas Wireless Propag. Lett.*, vol. 18, no. 6, pp. 1124–1128, Jun. 2019.
[32] M. M. M. Ali and A. Sebak, "Printed RGW circularly polarized differential feeding antenna array for 5G communications," *IEEE Trans. Antennas Propag.*, vol. 67, no. 5, pp. 3151–3160, May 2019.
[33] E. Baghernia, M. M. M. Ali, and A. R. Sebak, "2 × 2 slot spiral cavity-backed antenna array fed by printed gap waveguide," *IEEE Access*, vol. 8, pp. 170609–170617, 2020.
[34] B. Feng, J. Lai, K. L. Chung, T.-Y. Chen, Y. Liu, and C.-Y.-D. Sim, "A compact wideband circularly polarized magneto-electric dipole antenna array for 5G millimeter-wave application," *IEEE Trans. Antennas Propag.*, vol. 68, no. 9, pp. 6838–6843, Sep. 2020.

ELHAM BAGHERNIA (Graduate Student Member, IEEE) received the M.Sc. degree in electrical engineering from Ferdowsi University, Mashhad, Iran, in 2014. She is currently pursuing the Ph.D. degree in electrical engineering with Concordia University, Montreal, QC, Canada. She has been a Research and Teaching Assistant with the Department of Electrical and Computer Engineering, Concordia University, since 2016. Her current research interests include gap waveguide structures, microwave passive circuits and component, and millimeter-wave antennas.

REZA MOVAHEDINIA (Member, IEEE) received the Ph.D. degree in electrical engineering from Concordia University, Montreal, QC, Canada. He is currently a Research Engineer with Tallysman Wireless, Ottawa, ON, Canada. His current research interests include GPS/GNSS antennas, parasitic antennas, and millimeter-wave antenna arrays. He was a recipient of the International Tuition Award of Excellence and the Accelerator Award from Concordia University, in 2014 and 2016, respectively.

ABDEL-RAZIK SEBAK (Life Fellow, IEEE) received the B.Sc. degree (Hons.) in electrical engineering from Cairo University, Cairo, Egypt, in 1976, the B.Sc. degree in applied mathematics from Ain Shams University, Cairo, in 1978, and the M.Eng. and Ph.D. degrees in electrical engineering from the University of Manitoba, Winnipeg, MB, Canada, in 1982 and 1984, respectively. From 1984 to 1986, he was with Canadian Marconi Company, working on the design of microstrip phased array antennas. From 1987 to 2002, he was a Professor with the Department of Electronics and Communication Engineering (ECE), University of Manitoba. He is currently a Professor with the Department of Electrical and Computer Engineering, Concordia University, Montreal, QC, Canada. His research interests include phased array antennas, millimeter-wave antennas and imaging, computational electromagnetics, and interaction of EM waves with engineered materials and bio electromagnetics. He is a member of the Canadian National Committee, International Union of Radio Science (URSI) Commission B. He was a recipient of the 2000 and 1992 University of Manitoba Merit Award for Outstanding Teaching and Research, the 1994 Rh Award for Outstanding Contributions to Scholarship and Research, and the 1996 Faculty of Engineering Superior. He has served as the Chair for the IEEE Canada Awards and Recognition Committee, from 2002 to 2004, the Technical Program Chair for the 2002 IEEE CCECE Conference and the 2006 URSIANTEM Symposium, and the Technical Program Co-Chair for the 2015 IEEE ICUWB Conference.